https://doi.org/10.5194/egusphere-2022-329
Preprint. Discussion started: 20 June 2022

Mechanistic modelling of the variability of methane emissions from an artificial reservoir

Victor Lomov[1, 4, 5], Victor Stepanenko[1, 2, 3], Maria Grechushnikova[4, 6], Irina Repina[1, 3, 5]

[1]Laboratory of Supercomputer Modeling of the Earth system processes, Research Computing Center, Moscow State University, Moscow, Russia
[2]Meteorology and Climatology Department, Faculty of Geography, Moscow State University, Russia
[3]Moscow Center for Fundamental and Applied Mathematics, Moscow, Russia
[4]Hydrology Department, Faculty of Geography, Moscow State University, Russia
[5]A.M.Obukhov Institute of Atmosphere Physics, Russian Academy of Sciences, Moscow, Russia
[6]Institute of Water Problems, Russian Academy of Sciences, Moscow, Russia

Correspondence to: Victor Lomov (lomson620@mail.ru)

Abstract. We present the first mechanistic model LAKE2.3 for prediction of methane emissions from artificial reservoirs. Estimates of CH_4 emissions from the Mozhaysk reservoir (Moscow region) surface provided by the model are demonstrated. The annual emission value was 361 tC-CH_4 yr^{-1}, the average flux 37.7 mgC-CH_4 m^{-2} day^{-1}. The methane emission according to the model were shown to be in good agreement with the observation data. The ebullition makes the largest contribution to the total emission (up to 95 %). During the heating period, an increase of methane emission is observed both in the model and empirical data with a maximum before the onset of the autumn overturn. Effective parameter for calibrating the diffusion component of methane flux in the model is the potential rate of methane oxidation in the Michaelis-Menten reaction, and the same for ebullition is the temperature dependence parameter for methane production in bottom sediments – q10.

1. Introduction

The most important greenhouse gases in the atmosphere directly affected by anthropogenic emissions are carbon dioxide and methane. Methane is important, since its global warming potential per molecule is 72 times higher than that of carbon dioxide for 20 years period (Forster et al., 2007). In addition, the relative growth rates of methane content in the atmosphere significantly exceed those for CO_2 and N_2O: an increase in the average global surface methane concentration relative to the pre-industrial period is 167 % versus 46 % for CO_2 and 24 % for N_2O (IPCC, 2021).

There are natural and anthropogenic sources of methane in the atmosphere. The most important natural sources include wetlands, tropical forest ecosystems and lakes. Anthropogenic sources of methane in the atmosphere are landfills, agriculture, especially rice paddies and cattle pastures, industry, etc. (Sanuois et al., 2016). Artificial reservoirs are also a notable anthropogenic source of methane for the atmosphere.

The main source of methane in the water column of natural lakes and reservoirs is the anaerobic decomposition of organic matter in sediments (Fig.1). Even a small presence of oxygen in the bottom horizons can inhibit the activity of archaea - the main agents of organic matter (OM) anaerobic destruction (Tomaszek and Gruca-Rokosz, 2015). The dominating biogeochemical pathways of methane formation in sediments are hydrogenotrophic and acetoclastic reaction chains. Typically, in the upper part of the bottom sediments, the acetoclastic chain of OM decomposition prevails, and in deeper layers the hydrogenotrophic pathway provides the main contribution (Bazhin, 2003). The composition of the OM settling at the bottom sediments surface is important – with the arrival of labile (rapidly decomposing) organic matter, methane production is significantly accelerated (Whiticar, 2020).

https://doi.org/10.5194/egusphere-2022-329
Preprint. Discussion started: 20 June 2022

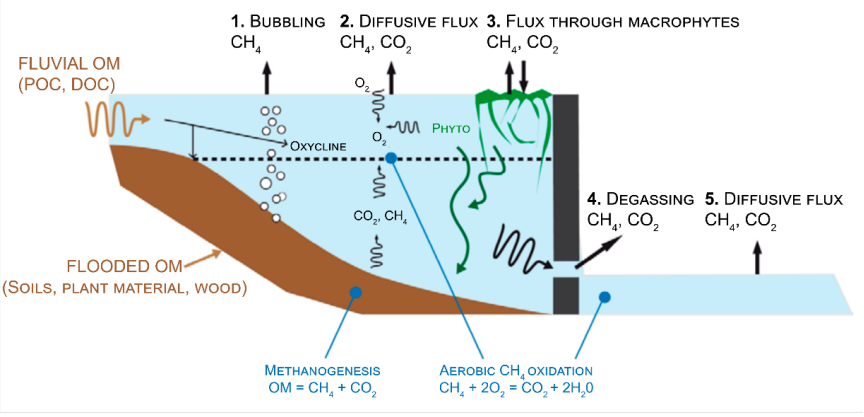

Figure 1: Distribution of methane fluxes and transformations in an artificial reservoir (Gash, 2010)

Methane produced in bottom sediments can reach the water-atmosphere interface in the aqueous form (diffusive flux of dissolved CH_4) or as a free gas in bubbles (ebullition process). In addition to the formation of methane directly in the bottom sediments, a significant contribution to the whole-lake CH_4 production can be provided by decomposition of macrophytes in shallow waters (Milberg et al., 2017). The diffusive flux depends on the dissolved methane concentration gradient, as well as the effective diffusion coefficient (including molecular and turbulent transport). When entering the oxygenated water layers, dissolved methane is oxidized by methanotrophic microorganisms, with a rate depending on concentrations of both methane and oxygen (Guerin and Abril, 2007). Up to 90 % of the diffusive flux can be oxidized between the oxycline and the water surface (Bastviken et al., 2008). Due to composition of above-mentioned factors, the CH_4 content increases from the surface to the bottom layers (Garkusha et al., 2016).

The key feature of ebullition flux is that it reaches the water surface much faster than the diffusive counterpart and cannot be directly oxidized. The bubble flux of methane depends on the local depth of the reservoir, as well as the water level dynamics. Artificial reservoirs are characterized by sharp level decrease during water flow regulation. A sharp drop in hydrostatic pressure at the bottom leads to increase of bubble volume in sediments (Harrison et al., 2017). The local reservoir depth affects the magnitude of the bubble flux due to dissolution of gas bubbles in the water column during their ascent, especially of large-diameter bubbles (Ostrovsky et al., 2008). With a smaller distance the bubble passes from the bottom to the surface, the fraction of gas molecules that have passed into the dissolved phase and subsequently oxidized in the oxycline is smaller (Miller et al., 2017).

An important factor, affecting the total methane flux from the reservoir to the atmosphere, is its trophic status. An increase in the phosphorus load to the reservoir, that leads to eutrophication process, and related amplification of chlorophyll content in the water lead to an increase of methane emissions from reservoirs by 30 – 90 % and may even bring lakes and reservoirs closer to swamps in terms of annual methane emissions into the atmosphere (Beaulieu et al., 2019). For eutrophic reservoirs, an essential seasonal increase in methane emissions takes place during the algae blooming period, when the rapid development of phytoplankton leads to a significant increase in primary production of OM (Bartosiewicz et al., 2021). At this time, the detritus sedimentation rate and hence the amount of incoming labile OM significantly increase, leading to rapid depletion of oxygen in the bottom layer, and supplying fresh substrate for anaerobic OM decomposition to methane.

In the inventory of methane emissions from reservoirs, it is important to take into account the horizontal components of the methane fluxes. A significant contribution to gross methane emissions from many reservoirs associated with hydroelectric power plants is provided by methane degassing in the water flow leaving the water body through the

https://doi.org/10.5194/egusphere-2022-329
Preprint. Discussion started: 20 June 2022

dam into the downstream. For deep reservoirs with small residence time, the methane output during degassing can account for up to 70 % of the total emission to the atmosphere (Kemenes et al., 2016).

According to available estimates, methane emissions from artificial reservoirs range from 2 to 122 Tg $year^{-1}$, or from 0.5 to 10 % of the total methane flux into the atmosphere from the Earth's surface (Deemer et al., 2016; Li and Zhuang, 2014; Louis et al., 2000; Tortajada et al., 2012; Tremblay et.al, 2005; Harrison et al., 2021; Rosentreter et al., 2021). Estimates of global methane emission from reservoirs vary significantly, due to the differences in assessment methodologies, as well as in the data sets involved. The assessment methods typically assume extrapolation of statistical relationships obtained for the multitude of studied objects to the rest (unexplored) reservoirs, using a set of predictors such as climatic zone, average depth, age, etc. (Tortajada et al., 2012). This approach, being useful for global estimates, may fail in prediction of methane emission from particular reservoirs and even regions.

A more reasonable methodology for estimating methane emissions from the surface of water bodies not covered by observations, or covered by a limited set of measurements, involves mechanistic modeling of the key processes of production, consumption, transport and emission of methane from a reservoir. The model needs to be tested and calibrated using the available empirical data on the spatial and temporal heterogeneity of methane fluxes in the water body of interest. After determining the optimal values of the model parameters and simulating the time series of methane fluxes at the water – atmosphere interface, it is possible to obtain refined estimates (inventory) of the annual methane flux for reservoirs, given their main morphometric, hydrological characteristics and atmospheric forcing.

One of the process-based models capable to perform such estimates is one-dimensional thermohydrodynamic and biogeochemical model LAKE (Stepanenko et al., 2016; Stepanenko et al., 2020). Models of this type have been previously used to estimate CH_4 and CO_2 emissions from natural lakes with high residence time (Stepanenko et al., 2011; Tan and Zhuang 2015; Tan et al., 2017a; Guseva et al., 2016; Tan et al., 2017b; Kiuru et al., 2018; Guseva et al., 2020). However, artificial water bodies are often characterized by significant horizontal heterogeneity in the distribution of both physical and biogeochemical variables, presenting a challenge for 1D models to successfully reproduce surface energy and mass exchange (Ishikava et al., 2021). Therefore, one of the objectives for this study is to assess the applicability of a 1D (vertical) approach to simulate the concentration and fluxes of methane in reservoirs using the LAKE model.

In this study, the Mozhaysk artificial reservoir (Moscow region, Russia) was chosen as an object to test a capability of the LAKE model to simulate methane fluxes and to apply a concept of improved inventory described above. The paper compares in-situ observed CH_4 concentrations and fluxes (as well as water temperature and dissolved oxygen) to results of the LAKE model and discusses possible ways to improve the quality of modeling and thus arriving to more accurate estimates of methane emissions from artificial reservoirs.

This paper includes an Introduction, providing a short overview of the processes responsible for methane fluxes in the water column and on the surface of the freshwater body; Materials and methods, describing the Mozhaysk reservoir, observation methods and results, as well as the LAKE model version 3, adopted for reservoirs with high throughflow and surface level variations; Results and discussion, presenting results of water temperature, oxygen and methane emission simulation by LAKE 3.0, comparison of simulations with empirical data, and quantification of the influence of selected factors on methane emission based on sensitivity experiments with the model.

https://doi.org/10.5194/egusphere-2022-329
Preprint. Discussion started: 20 June 2022

2. Materials and methods

2.1. Study site

The Mozhaysk artificial reservoir was used in this study as the site of field research and verification object for the LAKE model. This is a small morphologically simple (a reservoir without flooded valleys of large tributaries) valley reservoir in the Moscow region (55.5948 °N, 35.8221 °E) with a slow water exchange (Table 1).

Table 1: Morphological characteristics of the Mozhaysk reservoir (all characteristics are given for the mean headwater level) (Edelshtein, 2014)

Length, km	Max width, m	Mean width, m	Max depth, m	Area, km^2	Volume, km^3	Range of level fluctuations, m/year	Water residence time, year
28	2.6	1.1	22.6	30.7	0.24	6	0.6

To study the spatial heterogeneity of methane fluxes in the reservoir five reference observation stations were selected over the flooded riverbed (Fig.2). This arrangement of measurement stations at a uniform distance from each other in longitudinal direction of the reservoir facilitates the study of physical and biogeochemical characteristics distribution from upstream (affected by the tributaries) through the transformation zone in the middle course of the reservoir and to the lower part with a calm lake regime. In addition to observations over the flooded riverbed of the Moscow River, measurements were also carried out on other morphological sites within the selected reservoir compartments I – V (Fig. 2), namely, over the flooded floodplain of the river valley.

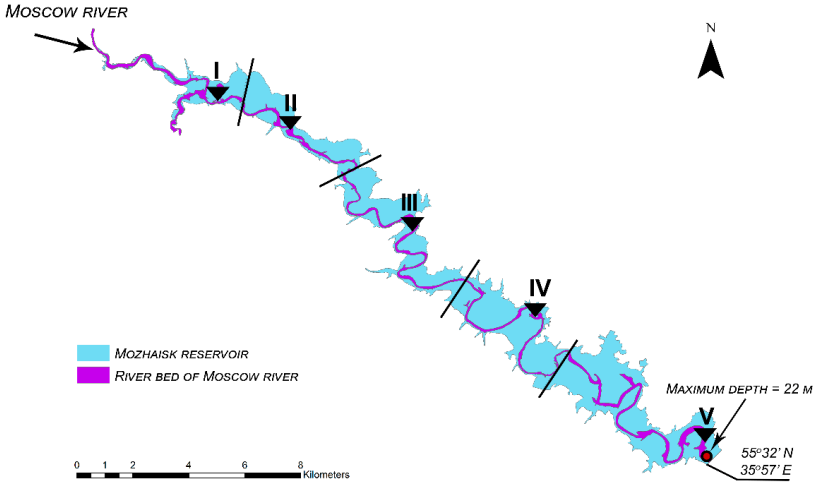

Figure 2: The scheme of the Mozhaysk reservoir with division into compartments according to the criteria of homogeneity of hydro-morphological conditions. The numerals I – V show reference stations for observation of methane concentrations and fluxes in 2015 – 2019

2.2. Field observations

The methane flux was measured by the floating chamber method (Gash, 2010; Bastviken et al., 2010). The method is based on measuring the concentration difference in the hermetic chamber, which is installed on the water, at the beginning and at the end of the exposure period. We used chambers of two types: a common chamber determining the

https://doi.org/10.5194/egusphere-2022-329
Preprint. Discussion started: 20 June 2022

sum of the bubble and diffusion flux, and a diffusion chamber, which is equipped by a screen that cuts off the bubble flux. The time of chamber exposition varied from 30 minutes to 1.5 hours. Water samples for detecting dissolved methane using the "headspace" method (Gash, 2010) were taken simultaneously with the measurement of methane fluxes by chambers. Samples were taken from the surface and bottom water horizons, as well as above and below the layer of the largest density gradient in the presence of stable temperature stratification. Sampling was accompanied by measurements of the water temperature, conductivity and dissolved oxygen with YSI ProODO and Pro30 probes. In addition, the air temperature, atmospheric pressure and wind speed were measured by Davis Vantage Pro meteorological suit at station IV which worked from May till September. Automatic measurements of water temperature were carried out at Station IV by temperature loggers at depths 0.5, 1, 2, 3, 4, 5, 7, 10 and 14 m every 15 min (Hobo pendant MX 2202 and Hobo Water Temperature Pro U22-001). Dissolved oxygen was measured by HOBO logger every 3 hours on surface layer (0.5 depth) and bottom layer (14 m), for vertical measurements YSI ProODO with 30 m cable was also used.

Measurements was divided on two types – measurements at all 5 stations (Fig.2) (carried out during one day) and more frequently temporal measurements on station IV (carried out on different time intervals, in some dates 2 – 4 times during the day) for more detailed information about temporal variability of methane fluxes and concentrations. Table 2 shows the dates of measurements. Measurements predominantly were carried out during the summer period of straight stratification.

Table 2: Dates of methane concentrations and fluxes measurements 2015 – 2019

Year	Measurements at all 5 stations	Additional flux measurements at station IV
2015	-	25.06; 29.06; 8.07-10.07; 28.07
2016	24.06; 4.07; 13.07; 22.08 Only concentrations	26.06; 27.06; 3.07; 9.07; 12.07; 27.07; 28.07; 21.08
2017	4.07; 5.07; 20.08 Only concentrations	20.06; 24.06; 27.06; 28.06; 3.07; 10.07; 28.07; 29.07; 31.07; 5.08; 19.08; 2.09; 9.09
2018	24.06; 7.07; 19.08	20.04; 9.05; 25.05; 17.06; 19.06; 26.06-29.06; 2.07; 8.07-10.07; 28.07; 17.08; 22.08; 28.07; 2.09; 8.09; 16.09; 21.09
2019	10.06; 24.06; 5.07	22.06; 23.06; 26.06; 2.07; 7.07; 9.07; 12.07; 12.08; 8.09
2020	25.05; 12.08	16.06; 24.06; 9.07; 12.09

To obtain more accurate measurement results, the errors of flux and concentration values was estimated. Relative error was calculated as a result of equivalent measurements series. During these measurements 3 – 12 successive samples of water methane concentration from the same location and depth and flux from the same chamber with 20 minutes intervals were taken. The results of this experiment showed, that the relative error have no relationship with value of the flux or concentration and no relationship with replication numbers. So, the maximum value of relative errors were applied as methods uncertainty estimation (Table 3).

Table 3: Experiment of relative error calculation for methane concentration and methane flux measurement

Type of measurements	Number of replications	Mean value	Relative error, %
Concentration	3	11.3 μLCH_4 L^{-1}	13.9
Concentration	**6**	**578.3 μLCH_4 L^{-1}**	**15.3**

https://doi.org/10.5194/egusphere-2022-329
Preprint. Discussion started: 20 June 2022

Concentration	8	18.7 μLCH$_4$ L^{-1}	1.8
Concentration	4	27.7 μLCH$_4$ L^{-1}	8.2
Concentration	5	18.0 μLCH$_4$ L^{-1}	2.2
Concentration	7	1165.5 μLCH$_4$ L^{-1}	13.9
Flux into atmosphere	**7**	**15.2 mgC-CH$_4$ m^{-2} d^{-1}**	**27.0**
Flux into atmosphere	7	3.09 mgC-CH$_4$ m^{-2} d^{-1}	25.0
Flux into atmosphere	12	6.74 mgC-CH$_4$ m^{-2} d^{-1}	25.7

The relative error values for measurements are 15.3 % for methane concentration and 27.0 % for methane flux.

2.3. Satellite measurements of water surface temperature

With the advent of medium- and high-resolution space scanners, it has become possible to detect various characteristics of any size inland water bodies (Palmer et al., 2015). A multispectral method using data from several satellite missions was used to determine the Mozhaysk Reservoir remote surface temperature. When constructing the reservoir mask, only those pixels that are reliably located on the water surface and do not capture areas of the shoreline were considered (Hosoda et al., 2007), and cloudy pixels were also excluded. The methodology for cloud pixel extraction is described in Schneider and Hook, 2010. Water temperature data from Landsat-8 satellite data were obtained using a two-channel algorithm (Aleskerova et al., 2016). This algorithm allows reconstructing the real surface water temperature. The Landsat-8 satellite carries the TIRS (Thermal InfraRed Sensor) instrument, which measures in two channels in the far infrared range (10.30 - 11.30 μm; 11.50 - 12.50 μm), which allows to provide atmospheric correction of measurements. The signal received by the satellite is the sum of signals from the water surface (temperature proper) and from the atmosphere (related to atmospheric transmittance). The emission characteristics of the atmosphere in the two channels are different, while the emission characteristics of the surface are the same (in the first approximation). Thus, the water surface temperature (T_w) according to Landsat-8 data can be calculated according to the following formula:

$$T_w = 1.911T_{10} - 0.8554T_{11} + 0.7837, \quad (1)$$

where T_{10} and T_{11} are temperatures obtained from channels 10 and 11 respectively. Calibrated temperature data from MODIS (Moderate Resolution Imaging Spectroradiometer) measurements were used to determine the coefficients. Sentinel-1 (2016) and Sentinel-3/SLSTR (2017) data were also used. The lake water temperature was calculated using the algorithm presented in (Carrea et al.,2015; MacCallum and Merchant, 2012). The surface temperature using the MODIS scanning spectroradiometer on the TERRA and AQUA satellite was determined using the methodology outlined in (MacCallum and Merchant, 2012). The L1C product of the MIRAS microwave radiometer (SMOS/ESA satellite) was also used to obtain the seasonal dynamics of the brightness temperature of the cell corresponding to the reservoir. Periods of characteristic open water and ice cover brightness temperature values were identified (Tikhonov et al., 2018).

2.4. Description of the LAKE model

The LAKE is a one-dimensional (with a partial representation of horizontal inhomogeneity) thermohydrodynamic model of a water body with a module of biogeochemical processes responsible for the formation of methane and carbon dioxide (https://mathmod.org/lake/). Relevant model code and all scripts can be found on “zenodo” data base (https://zenodo.org/record/6353238#.YqjVDRlBxPY). The model has been used previously to simulate the

https://doi.org/10.5194/egusphere-2022-329
Preprint. Discussion started: 20 June 2022

thermodynamic regime of reservoirs, as well as the CO_2 (Iakunin et al., 2020) and CH_4 (Stepanenko et al., 2020) dynamics. A version of the model LAKE2.3 summarized below was used to estimate the CH_4 flux from the reservoir. This section provides a general description of the mathematical model with links to publications where individual modules are given in more detail. Particular attention is paid to the representation of physical mechanisms and biogeochemical effects associated with the water flow through the reservoir, since their representation mainly distinguish the 2.3 version of the model from the preceding ones.

The one-dimensional (in vertical) equations for thermodynamic, dynamic and biogeochemical variables in a reservoir are the result of an averaging operation over the horizontal section of a water body (Fig. 3) applied to three-dimensional equations for horizontal momentum components, the continuity equation, the heat equation, the dissolved/solid species balance equations.

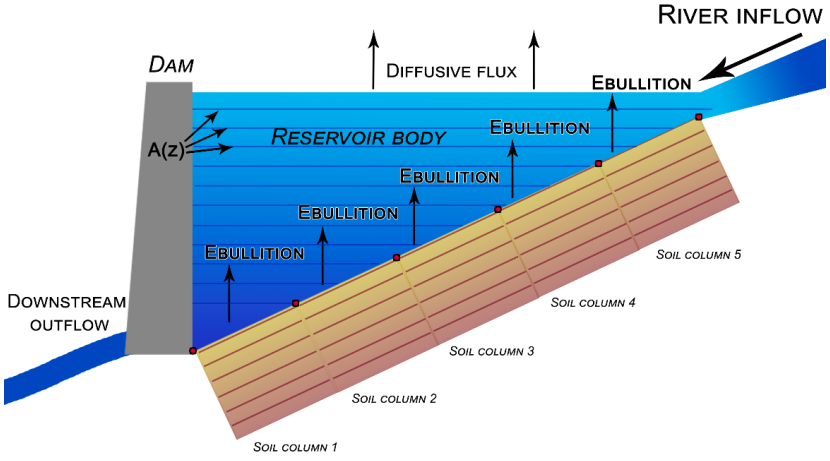

Figure 3: Discretization of the water body and bottom sediments in the LAKE 2.3 model. Blue lines show horizontal sections (of the area A(z)) of the reservoir at the levels of the model finite-difference scheme, bright brown boxes depict columns of bottom sediments located at different depths of the reservoir, brown lines standing for model levels in sediments

The resulting form of a one-dimensional equation for a scalar value f (including any of the horizontal velocity components u, v) in an incompressible fluid has the form:

$$\frac{\partial \bar{f}}{\partial t} = -\frac{1}{A}\oint_{\Gamma_A} f\boldsymbol{u}\cdot\boldsymbol{n}\,dl - \frac{1}{A}\frac{\partial A\overline{w}\bar{f}}{\partial z} + \frac{1}{A}\frac{\partial}{\partial z}\left[A(k_T + k_m)\frac{\partial \bar{f}}{\partial z}\right] - \frac{1}{A}\frac{\partial A\bar{\Phi}_f}{\partial z} + \frac{1}{A}\frac{dA}{dz}\left(F_{f,\Gamma_{A(z)}} + \Phi_{f,\Gamma_{A(z)}}\right) + \bar{R}, \quad (2)$$

where z – the vertical coordinate directed along gravity, with the origin at the water surface, t – time, $A(z)$ – the horizontal section, $\Gamma_{A(z)}$ – the closed boundary of the section A(z), dl – the element of the $\Gamma_{A(z)}$ boundary length (Fig. 3), n – the external normal to $\Gamma_{A(z)}$, $\boldsymbol{u} = (u, v)$ – the horizontal component of velocity, w – the vertical projection of velocity, F_f – the total diffusion flux of f due to turbulence and molecular exchange, Φ_f – the sum of non-diffusion and non-advective fluxes of f (for example, radiation flux in the equation for temperature, bubble flux in the equations for dissolved gases), $F_{f,\Gamma_{A(z)}}$, $\Phi_{f,\Gamma_{A(z)}}$ – values of the corresponding fluxes at $\Gamma_{A(z)}$, i.e. at the bottom of depth z (within $\Gamma_{A(z)}$ these fluxes are assumed to be constant), R – the sum of all terms of the original three-dimensional equation, except for the total derivative and divergence of fluxes (i.e. sources and sinks in the equations for biogeochemical substances, pressure gradient and Coriolis force in the equations of motion, etc.), overbar $\overline{(\ldots)}$ stands for horizontally averaged expression.

https://doi.org/10.5194/egusphere-2022-329
Preprint. Discussion started: 20 June 2022

Equation (2) is valid for the case of a bottom with small slopes (so that horizontal components of diffusion fluxes and vertical velocity at the bottom are negligible), as well as for a reservoir formed by vertical walls with zero normal diffusion fluxes and a horizontal bottom. In the context of this study of a water flow through reservoir, the first and second terms in the right-hand side of (2) are of particular interest, since they are responsible for the inflow by the tributaries and removal by discharge of the value f and for advection of f by the average vertical velocity, respectively. The equations in the form (2) are solved in the model for the following variables:

- horizontal speed components;
- temperature;
- salinity (mineralization);
- concentration of dissolved oxygen, methane;
- concentration of carbon atoms in the following forms: living organic particles (phyto- and zooplankton), dead organic particles (detritus), autochthonous and allochthonous dissolved organic carbon, dissolved inorganic carbon;
- concentration of phosphorus atoms of the dissolved inorganic phosphorus (phosphates).

Equations of the form (2) are supplemented by boundary conditions at the upper and lower boundaries. For temperature, the heat balance equation is used at the upper boundary ($z = 0$) and the continuity of temperature and heat flux at $z = H$ (H is the maximum depth of the reservoir). The heat balance on the surface is calculated under given time series of short-wave and long-wave radiation fluxes and basic meteorological parameters; the turbulent fluxes of sensible, latent heat and momentum are calculated using the Monin-Obukhov similarity theory (Businger et al., 1971; Paulson, 1970).

The equation for the mean vertical velocity is obtained by averaging over the horizontal cross-section of continuity equation:

$$\frac{\partial A\bar{w}}{\partial z} = -\oint_{\Gamma_A} \boldsymbol{u}\cdot\boldsymbol{n}\, dl, \tag{3}$$

given the impermeability condition $\bar{w}|_{z=H} = 0$.

Integrating (2) and taking into account water fluxes at the surface, the equation for H is obtained:

$$\frac{dH}{dt} = r - E - \frac{1}{A(0)}\int_0^H \oint_{\Gamma_A} \boldsymbol{u}\cdot\boldsymbol{n}\, dl\, dz + M, \tag{4}$$

which expresses the change in the water level as a result of the inequality of the discharges of inlets and outlets, precipitation r, evaporation E from the surface, as well as the processes of freezing and melting of ice and snow cover (represented by the summand M).

The system consisting of one-dimensional equations of the form (2) and the continuity equation (3) is closed using additional hypotheses and parameterizations (Stepanenko et al., 2016). Thus, the turbulent closure k-ε is used to calculate the coefficients of turbulent viscosity and thermal conductivity (diffusivity); the expression for the coefficient of thermal conductivity (diffusivity) also includes the additive coefficient of "background diffusion", representing vertical mixing due to the internal waves breaking and other mixing effects not accounted for in standard turbulent closures. Parameterizations of the fluxes of scalar quantities and momentum at the bottom surface $F_{f,\Gamma_{A(z)}}, \Phi_{f,\Gamma_{A(z)}}$ at $z < H$ also play an important role. Heat and methane fluxes at the bottom are calculated by solving one-dimensional problems for temperature and methane in layers (columns) of bottom sediments having a boundary with water body at different depths (Stepanenko et al., 2016), including the maximum depth, so that the sum of these boundaries is the entire bottom area of the reservoir (Fig. 3). Momentum flux through the bottom surface $\left(F_{u,\Gamma_{A(z)}}, F_{v,\Gamma_{A(z)}}\right)$ is calculated according to the linear or quadratic law in respect to average velocity $(\bar{u}, \bar{v})$ with a calibration multiplier.

https://doi.org/10.5194/egusphere-2022-329
Preprint. Discussion started: 20 June 2022

The one-dimensional model of heat and moisture transfer in bottom sediments takes into account the possibility of phase transitions of water. The equation for methane concentration in sediments includes production, molecular diffusion, and removal of methane in the form of bubbles when the critical CH_4 concentration is exceeded (Stepanenko et al., 2011).

Non-diffusive and non-advective fluxes Φ_f – are the kinematic shortwave radiation flux $\Phi_T = S$ in the heat equation (computed according to the Beer-Buger-Lambert law for the infrared, photosynthetically active, near and far infrared wavelength ranges) and the bubble flux in the equations for the concentrations of dissolved oxygen, carbon dioxide and methane. The bubble model is based on parameterizations from (McGinnis et al., 2006) and takes into account the exchange of five gases between the water and the bubble: O_2, CO_2, CH_4, N_2, Ar.

A separate task is to construct parametrizations for the terms $\bar{R}$ in one-dimensional models. Thus, parameterization of the averaged horizontal pressure gradient in the momentum equations in the LAKE model allows to reproduce seiches with horizontal wave number 1 (Stepanenko et al., 2020). Sources and sinks $\bar{R}$ in the equations for biogeochemical substances are set using parameterizations from Fang and Stefan, 1994; Hanson et al., 2004; Tan et al., 2017a; Sadeghian et al., 2018; Fichot and Miller, 2010; Koehler et al., 2014 and take into account the following processes:

- photosynthesis, respiration, exudates and death of phyto- and zooplankton;
- aerobic decomposition of dissolved organic compounds and detritus;
- photochemical decomposition of dissolved organic compounds;
- aerobic oxidation of methane.

The consumption of dissolved oxygen by bottom sediments with the release of dissolved inorganic carbon and dissolved inorganic phosphorus are expressed by terms $F_{f,\Gamma_{A(z)}}$ in the balance equations of these variables according to (Walker and Snodgrass, 1986).

The one-dimensional model with a partial representation of horizontal inhomogeneity presented above allows to calculate the following fluxes of gases into the atmosphere:

- diffusion flux from the surface of the reservoir (the gas exchange coefficient is provided according to the surface renewal model (Donelan and Wanninkhof, 2002));
- bubble flux calculated separately above bottom sediments located at different depths (Fig. 3);
- advective flux through the outflow (or turbines in the case of hydroelectric power plants).

The model includes multilayer modules for calculating the transfer of heat and liquid moisture in layers of ice and snow (Stepanenko et al., 2019).

The system of the model equations is solved by finite-difference methods.

2.5. Setup of numerical experiments

The input data to the model is divided into hydrological information (discharge of water, heat, momentum and water constituents by main tributaries, water level or discharge through a dam) and meteorological forcing (temperature, humidity, atmospheric pressure, wind speed, shortwave and longwave radiation, precipitation). Water level data was extracted from Mozhaysk Hydroelectric Power station archive, ERA5-Land reanalysis was used as a source of meteorological data. These meteorological data were corrected according to the available series of ground observations both at the reservoir and at the nearest meteorological stations Mozhaysk and Naro-Fominsk (Lomov et al., 2020b). Data corrected for all modelling period of 2015 – 2019.

The baseline numerical experiment with the LAKE model was carried out for the period from 2015 to 2019, whereas the period November - December 2014 was used as the model spinup period. The time step of the model finite-

https://doi.org/10.5194/egusphere-2022-329
Preprint. Discussion started: 20 June 2022

difference scheme was set 10 seconds, the step of meteorological data was 1 hour, the input hydrological information was updated daily. The water temperature observed in the fall of 2014 was taken as the initial conditions, the oxygen saturation degree at the initial moment was set to 100 %, which is realistic for the autumn well-mixed homothermy stage. The initial methane concentration was set to 0, since no corresponding observations were available at that time. 22 horizontal levels were set in the model with approximate spacing of 1 m, which corresponds to the maximum depth of the reservoir at the initial instant, 5 columns of bottom sediments evenly distributed over the depth of the reservoir, each 1 m thick, with the grid step inside each column 10 cm.

Model parameters were measured *in situ* where possible or set up according to literature data. For example, the extinction coefficient of solar radiation, was set as constant according to Secchi disk measurements on the reservoir equals 1.4 m^{-1}. The coefficient of additional diffusion in the thermocline is important for the correct simulation of the diffusive heat flux in metalimnion with stratification strong enough to cause turbulent moments vanishing in standard turbulence closured (including k-ε closure used in LAKE model). This coefficient is semi-empirical and is expressed by the formula:

$$k_{BD} = k_0 A_0^{k_1} (N^2)^{-k_2}, \quad (5)$$

where k_0 = 8.17E-4, k_1 = 0.56, k_2 = -0.43 are empirical coefficients, A_0 is the water surface area and N is the Brunt-Väisälä frequency (Stepanenko et al., 2016; Hondzo et al., 1993).

3. Results and Discussion

3.1. Methane emission by *in situ* measurements

The greatest temporal variability of methane fluxes from Mozhaysk reservoir is typical for the summer season (Fig. 4). Information on this variability was collected during observations conducted at station IV (Fig. 2) for the period 2015-2019.

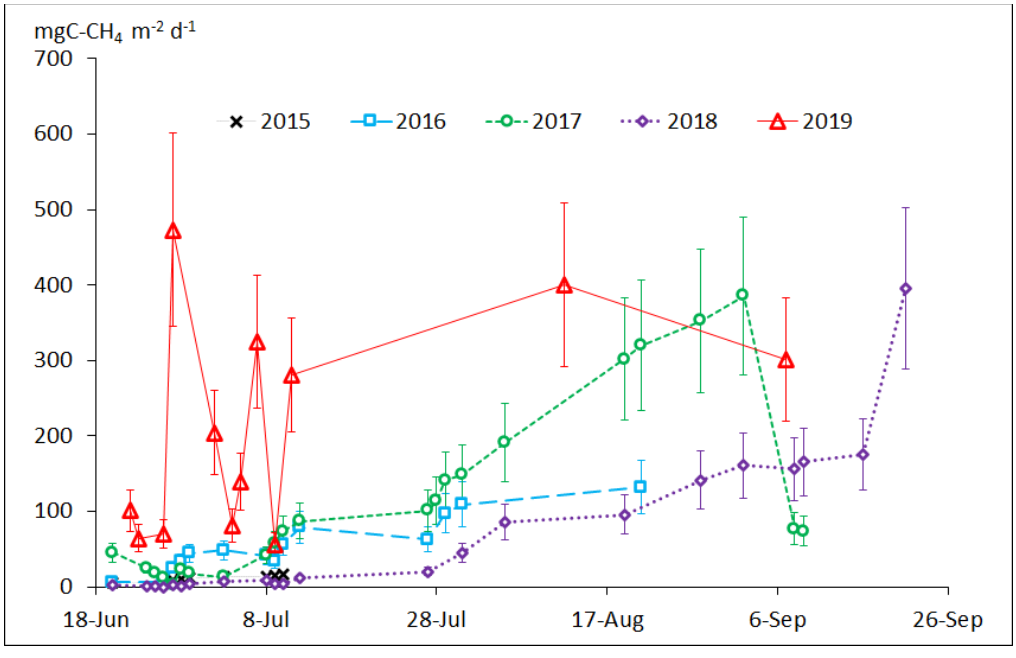

https://doi.org/10.5194/egusphere-2022-329
Preprint. Discussion started: 20 June 2022

Figure 4: Total methane flux into the atmosphere from the reservoir surface at station IV (Fig. 2); the whiskers show the 27 % confidence intervals

For most years, there is a similar tendency of enhancing the methane flux during summer (2016-2018). The maximum flux value is typically reached at the end of summer period, i.e. at the commence of the autumn convection. By this time, a thick anaerobic zone with dissolved O_2 content of less than 1 mg L^{-1} is formed in the hypolimnion due to the stable temperature stratification (Lomov et.al., 2020a). This favors methane accumulation in the bottom layers of water. In addition, by the end of summer, the productivity of the reservoir significantly increases, and a large amount of dead organic matter (detritus) subsides to the bottom sediments thus adding a substrate for anaerobic destruction (in agreement with established link of trophic status to methane emissions (Beaulieu et al., 2019)). This in turn contributes to a significant increase of the total methane flux. At high values of the total methane flux, the ebullition flux can account for more than 90 % of the total emission (Lomov et.al., 2020a). It is worth noting that the increase of CH_4 flux during summer may occur gradually (as in 2017, when the temperature stratification was weak), or include a sharp release of methane when a stable temperature stratification took place (as at the end of the summer 2018).

First step of methane emission estimation was to estimate the flux from riverbed morphometric part of reservoir. Quasi-synchronous (conducted during 1 day) observations on flooded riverbed reservoir part of total methane flux in different parts of the Mozhaysk reservoir (stations I – V) (Fig. 2) were carried out in the summer periods of 2018 – 2020. The average ratio of CH_4 flux at riverbed station IV to the zonally averaged flux from the entire riverbed reservoir area was calculated basing on the results of all the surveys (Fig. 5a).

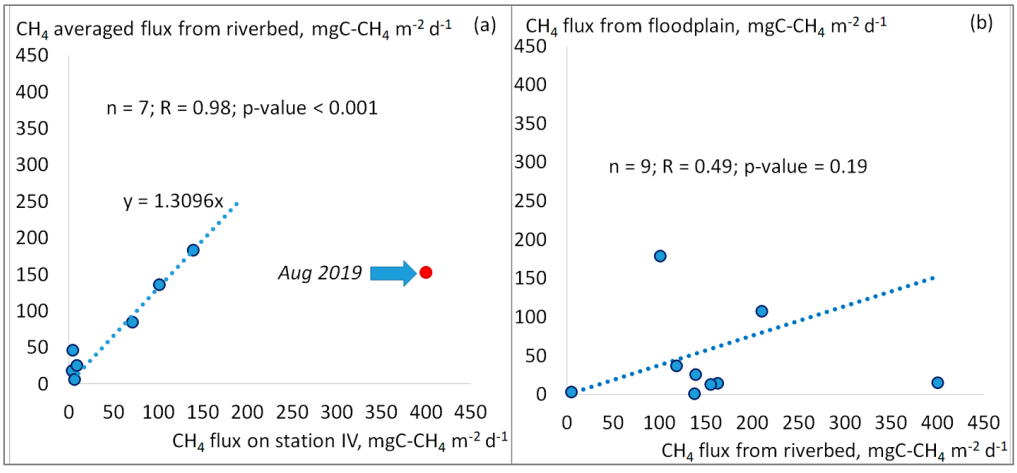

Figure 5: The scatter plot for the spatial-averaged total CH4 flux from the entire riverbed area of Mozhaysk reservoir and the CH4 flux at riverbed station IV (a), the scatter plot for CH4 flux above the flooded riverbed and the flux above the flooded floodplain (b) according to quasi-synchronous (conducted during 1 day) measurements

For horizontal averaging of CH_4 riverbed flux, the areas of the reservoir compartments (Fig. 2) were used. For each compartment, a methane riverbed flux value was assigned from the corresponding observation station (Fig. 2). Then the following regression was assumed between methane riverbed flux averaged on all Mozhaysk reservoir and methane flux on station IV. Thus, the multiplier 1.3 was used to estimate the total emission from the entire riverbed area of the reservoir by the values of CH_4 flux obtained at station IV only, where the flux on flooded river channel was measured more often (61 measurements at station IV versus 8 whole-reservoir surveys). However, at the Fig. 4a one value (August 2019) is significantly out of the general pattern. This is due to very low water level of the reservoir in August 2019, at which the spatial distribution of methane fluxes differs greatly from the distribution observed

https://doi.org/10.5194/egusphere-2022-329
Preprint. Discussion started: 20 June 2022

during the typical water levels; therefore, at water levels below 179 m (Baltic Elevation System), the mentioned conversion multiplier from value at station IV to entire riverbed reservoir area was assumed 0.4.

The values of methane fluxes considered above refer to the flooded river channel of the Mozhaysk reservoir, since all main measurement stations (Fig. 2) were located in the deepest points of sections. The second step of emission calculation is to relate the values, obtained for riverbed part with floodplain part of Mozhaysk reservoir. A number of quasi-synchronous measurements were carried out in each compartment and at different periods above the riverbed and above the floodplain in the same reservoir section (Fig. 5b) in order to take into account inundated floodplain areas, which have smaller depths and larger areas. The ratio of methane fluxes over the riverbed and floodplain differs significantly in all sections and between periods. There is no significant relationship between riverbed and floodplain methane fluxes. However, based on the fact that the entire water area of the Mozhaysk reservoir was covered by these synchronous measurements, the average ratio of the floodplain flux to the riverbed flux for all measurements was taken as a conversion factor, which was assumed 0.38.

Thus, based on the temporal variability of methane fluxes at station IV using the quantitative relationships of fluxes in different parts of the reservoir described above, we computed the time series of zonaly averaged values of the total methane flux from the surface of the Mozhaysk reservoir based on measurements at station IV. These time series were linearly interpolated between measurements at station IV to get series with daily resolution. The averaged fluxes of daily resolution were multiplied by the area of the Mozhaysk reservoir for each day, thus obtaining the value of the daily methane emission. The sum of daily emission values provided the annual methane emission from the surface of the Mozhaysk reservoir.

The emission of methane during degassing in the downstream of the hydroelectric powerplant was estimated as degassing through turbines. It was calculated as the difference in methane concentrations in the horizon of water intake in the upstream and downstream multiplied by the turbine discharge (Kemenes et al., 2016). Thus, the values of total methane emissions during summertime for 2017-2019 (less measurements data of the methane flux during summer period of 2015 and 2016 doesn't allow to estimate emission these years) from the Mozhaysk reservoir were obtained (Table 4).

During the ice period methane emission is assumed zero; in spring and autumn, when the reservoir is characterized by homogeneity of temperature and dissolved/solid substances, low water temperature values and low productivity, the methane flux is set to a value 2.4 $mgC\text{-}CH_4\ m^{-2}\ day^{-1}$, which is the mean value of several observations during these periods in different years (September 2017, April 2018).

Table 4: Estimates of the annual methane emission from the Mozhaysk reservoir for 2017-2019 according to field observations

year	Emission from the water surface, $tC\text{-}CH_4$	Degassing through turbines and downstream, $tC\text{-}CH_4$	Total emission, $tC\text{-}CH_4$
2017	334	13	347
2018	256	9	265
2019	378	11	389

3.2. Thermodynamic, oxygen, methane concentration regime and methane emissions according to the LAKE model

The quality of the model simulations was assessed in terms of 4 variables – water temperature, dissolved oxygen, dissolved methane and methane fluxes at the water-atmosphere interface. The results of the LAKE model were

https://doi.org/10.5194/egusphere-2022-329
Preprint. Discussion started: 20 June 2022

compared with observations conducted during summers of 2016-2019 period at station IV. Excepting the total emission estimations, which were compared to already averaged values (see Section 3.1).

3.2.1. Temperature regime

The simulated water temperature time series were compared with the loggers data from depths 0.5, 1, 2, 3, 4, 5, 7, 10 and 14 m at station IV. The model reproduces the temperature variability in the upper mixed layer well enough, both at diurnal and seasonal scales (Fig. 6).

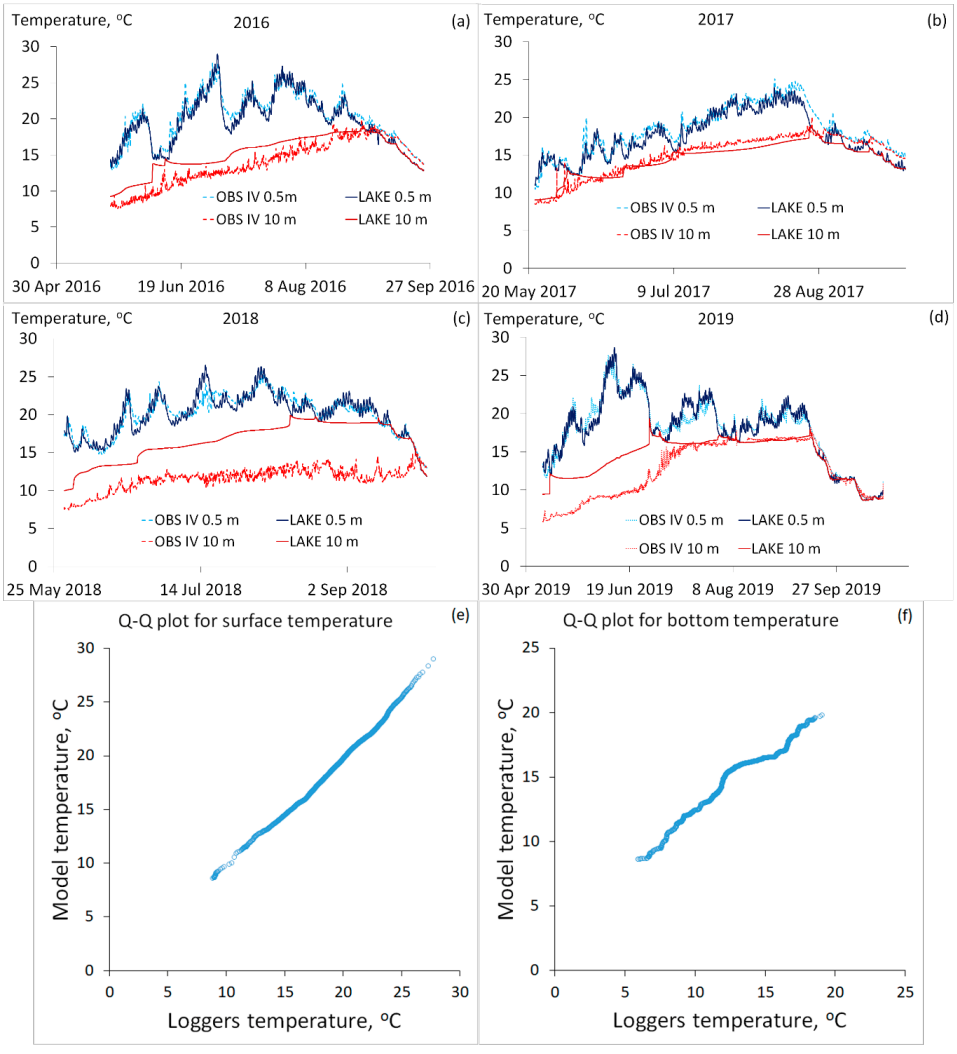

Figure 6: Time series of water temperature in the surface mixed layer and at 10 m depth, measured at station IV of Mozhaysk reservoir and simulated by LAKE model. Subfigures (e) and (f) shows the Q-Q plots between measured and simulated temperatures for surface and bottom layers respectively

Table 5 shows the difference in mean values between calculated by model and measured data and also the statistical criterias of data convergence for model temperature calculation quality. Pearson R and Nash-Sutcliffe Efficiency (NSE) (Nash and Sutcliffe, 1970) was used as statistical criterias.

https://doi.org/10.5194/egusphere-2022-329
Preprint. Discussion started: 20 June 2022

Table 5: Statistical criterias for comparison of water temperature between model calculations and in situ measurements

Surface layer				10 m layer			
year	Difference in mean, ºC	Pearson R	NSE	year	Difference in mean, ºC	Pearson R	NSE
2016	-0.54	0.97	0.91	2016	1.32	0.91	0.64
2017	-0.84	0.96	0.86	2017	-0.51	0.96	0.86
2018	-0.01	0.92	0.84	2018	4.26	0.64	-16.16
2019	0.00	0.98	0.95	2019	2.07	0.78	0.21
Average	-0.34	0.96	0.91	Average	1.77	0.66	0.11

The temperature at 10 m depth is reproduced by the model less successfully and strongly depends on the conditions of a particular year. The best results were obtained for 2017 and 2016, while in 2018 and 2019 the model provides more intense seasonal vertical heat trasnport to deep layers compared to observed temperatures. The vertical heat transport in the metalimnion in the model is substantially governed by coefficient of background thermal conductivity of a simplified form (formulae 2), which does not allow mixing in metalimnion to be reproduced equally well under atmospheric forcing of different years. Figure 6 also demonstrates high-frequency oscillations of temperature at 10 m in observed series, presumably originating from internal waves, not reproduced in the 1D model, as seiche oscillation parameterization (Stepanenko, 2016) was switched off in this study.

LAKE model reproduce the avereged water layer temperature due to 1D scale. So, the model surface layer calculations was also compared with satellite observations described in section 2.3 of this article. Satellite data allow to obtain averaged temperature data that can be averaged over reservoir surface in contrast to station measurements. Water surface temperatere obtained by LAKE model and satellite measurements for 2016 – 2017 showed on Figure 7.

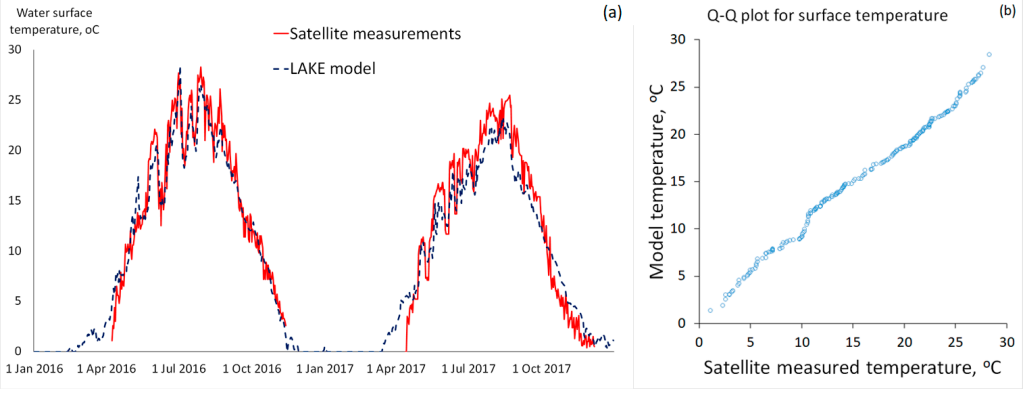

Figure 7: Comparison between model water surface temperature and satellite observations (a) and Q-Q plot between satellite measured surface water temperatures and simulated surface temperatures (b)

Model water surface temperature has even better data convergence with satellite observations than with *in situ* measurements. In general, model results of water surface temperatures calculation are lower then the satellite data for 0.67 degrees for 2016 – 2017 period. Statistical criterias showed in Table 6.

Table 6: Difference in mean values and statistical criterias for comparison of water surface temperature between model calculations and satellite observations

year	Difference in mean, ºC	Pearson R	NSE
2016	-0.48	0.97	0.98

https://doi.org/10.5194/egusphere-2022-329
Preprint. Discussion started: 20 June 2022

2017	-0.84	0.98	0.97
Average	-0.67	0.97	0.97

3.2.2. Dissolved oxygen regime

During summer, the measured dissolved oxygen concentrations in surface water layer were significantly higher than those provided by the model (Fig. 8a). In the LAKE model, the daily-averaged parameterization scheme of the carbon cycle processes is adapted from Hanson et al., 2004, therefore, the daily cycle of O_2 content in surface layer is reproduced with suppressed amplitude. In the model oxygen concentrations is in close equilibrium with the atmospheric O_2 content, that cause underestimation. The smallness of deviations from the equilibrium state are explained by the approximate equality of sources (photosynthesis) and sinks (respiration, decomposition of dead organic matter) in the modeled epilimnion. In turn, this may be caused by the high rate of detritus oxidation, which does not leave time for detritus to sediment from the mixed layer due to gravitational deposition. However, significant model error in the O_2 concentration does not matter for simulated methane oxidation rate in the surface layer. Oxygen concentrations of ~ 6-14 mg L^{-1} is too high for limitation of the methanotrophic bacteria activity. In other words, both in the model and in the observations, the oxygen content in the mixed layer significantly exceeds the half-saturation constant 0.33 mg L^{-1} for O_2 in the Michaelis-Menten kinetics of CH_4 oxidation, used in LAKE.

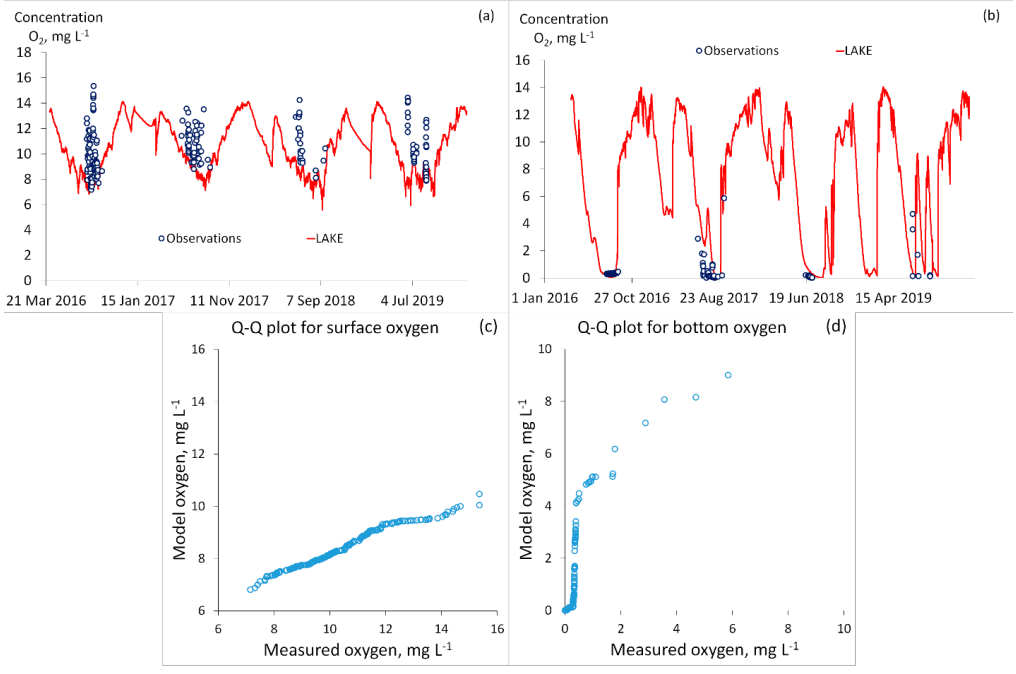

Figure 8: Time series of dissolved oxygen concentration in the surface mixed layer (a) and in the bottom water layer (14m) (b) measured at station IV of Mozhaysk reservoir and simulated by the LAKE model in 2016-2019. Subfigures (c) and (d) shows the Q-Q plots between measured and simulated oxygen concentrations for surface and bottom layers respectively

For the processes of methane accumulation in hypolimnion which are important for CH_4 flux formation, a crucial variable is the oxygen content in the bottom layer, especially during the formation of an anoxic zone. The model satisfactorily reproduces the observed O_2 content at 14 m depth at station IV during all years, where such measurement data is available (Fig. 8b).

https://doi.org/10.5194/egusphere-2022-329
Preprint. Discussion started: 20 June 2022

The statistical criterias (Pearson R and NSE) was not calculated for comparison between regular *in situ* measurements on station IV and model results, due to unregular temoral frequancy of these measurements. Also, in some periods (for example summer 2019 bottom oxygen concentration measurement) there are only 7 field measurements, that is not enough for statistical approach. Only difference in mean was calculated for the period 2016 – 2019. For surface layer average value of *in situ* measurements is 10.08 mg L^{-1} and the mean of calculated values is 8.40 mg L^{-1} model concentrations are lower by 2.08 mg L^{-1}. For bottom water layer average value of *in situ* measurements is 0.39 mg L^{-1} and the mean of calculated values is 1.26 mg L^{-1} (difference in mean is 0.87 mg L^{-1}).

In parallel with single measurements, the oxygen concentration in water was obtained by logger gauges, described in section 2.2. The comparison between model results and oxygen loggers showed in Figure 9.

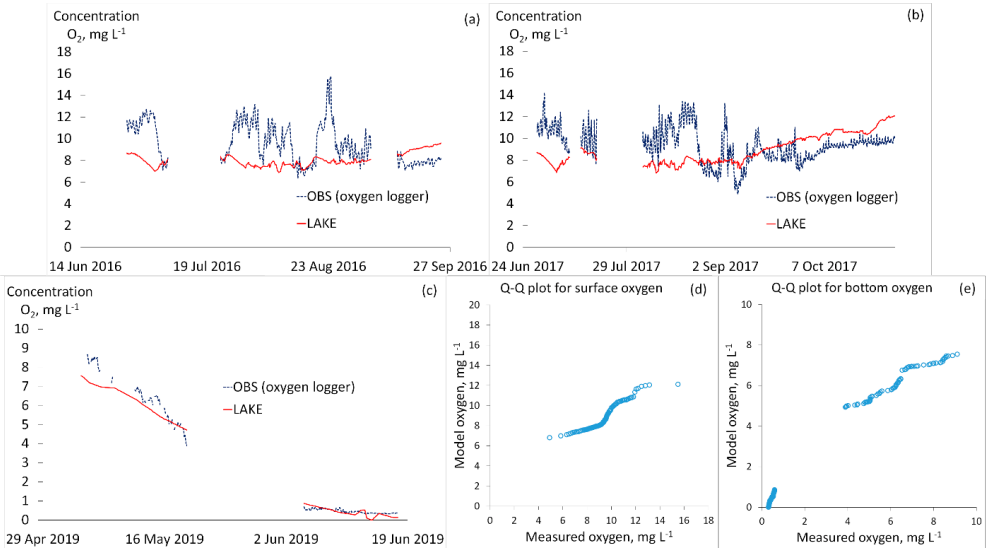

Figure 9: Time series of dissolved oxygen concentration obtained using high-frequency oxygen gauges – surface oxygen concentration in summer period of 2016 (a), surface oxygen concentration in summer period of 2017 (b), bottom oxygen concentration in summer period of 2019 (c) and LAKE model oxygen calculation. Subfigures (d) and (e) shows the Q-Q plots between measured and simulated oxygen concentrations for surface and bottom layers respectively

The results of such comparison is the same – model calculate the surface oxygen concentrations lower, than gauge measurements, but for bottom water layer there are strong convergence between logger data and model (Table 7).

Table 7: Difference in mean values and statistical criterias for comparison of oxygen content between model calculations and observations

year	Difference in mean, mgO_2 L^{-1}	Pearson R	NSE
2016 (surface)	-1.67	-0.26	-1.04
2017 (surface)	-0.30	-0.03	-0.94
2019 (bottom)	-0.34	0.99	0.97

3.2.3. Methane concentration in water

The LAKE model reproduces satisfactorily the observed temporal variability of the mixed-layer CH_4 concentration, however, overestimates the measured values on average by 0.3 - 0.5 µmol L^{-1} (Fig. 10). It can be partially related with spatial variability of methane concentration. Observations showed (measurements at 5 stations described in section 2.2), that methane surface concentrations can vary in 0.2 – 0.3 µmol L^{-1} between upper and lower parts of reservoir (stations I and V on Figure 2). Compared to CH_4 observations at the bottom layers at station IV, the LAKE model

https://doi.org/10.5194/egusphere-2022-329
Preprint. Discussion started: 20 June 2022

460 demonstrates the lower rate of methane accumulation in hypolimnion (Fig. 10b). However, seasonal concentration maxima coincide in the same time according to observations and to LAKE model. For comparison, Figure 10b shows the time series of methane concentration not only at a depth of 14 m (local depth of the station IV), but also at the lower model layer – 22 m (maximal depth of the reservoir). Even at the deepest horizon in the model, methane accumulates less intence than what observed at the local depth of station IV. The reason for this discrepancy between
465 model and observations is likely to be twofold. First, 1D lake model by construction simulates areally averaged CH_4 concentration which should be lower than the methane content at the bottom, where the gas has its source. And second, the suggested link between mixed-layer productivity and methane production in sediments through sedimenation of detritus (see Section 3.1) is not represented in current version of LAKE model.

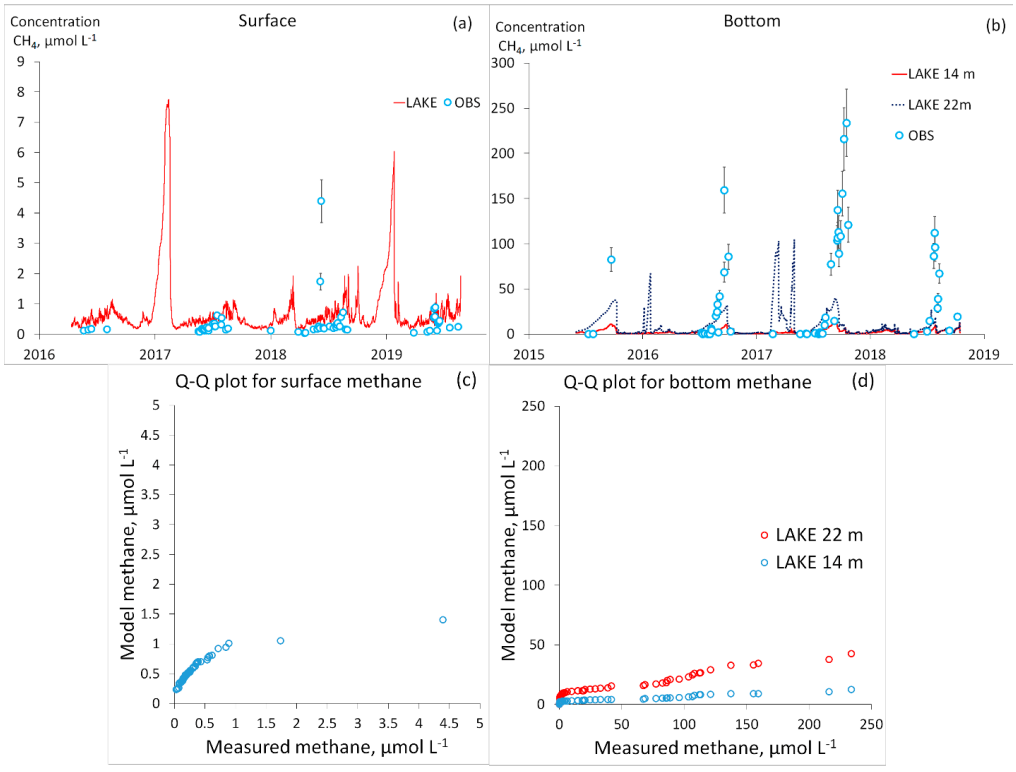

470 **Figure 10: Time series of methane concentration in the surface mixed layer, according to measurements at station IV and LAKE simulations (a), and at the local depeest point of station IV (14 m), observed and modeled, and maximal reservoir depth (22 m, simulated only) (b). Subfigures (c) and (d) shows the Q-Q plots between measured and simulated methane concentrations for surface and bottom layers respectively. For observations, values are given at intervals corresponding to the relative error in determining the methane concentration 15.3 %**

475 **3.2.4. Methane fluxes into the atmosphere**

The time series of the diffusion and ebullition methane fluxes averaged over the surface of Mozhaysk reservoir simulated by LAKE are given at Figure 11. The main contributor of methane emission is ebullition – during the periods of maximum fluxes it can contribute up to 95 % of total emission into the atmosphere. The second component of the flux is diffusive emission, and the lowest values calculated by methane degassing through turbines. During the
480 winter period the values of all 3 flux types is low, values more than 10 mgCH_4 m^{-2} d^{-1} can occur when the ice cover weakens. High emissions can occur in early spring, when the ice cover melted totally (up to 302 mgCH_4 m^{-2} d^{-1} 01

https://doi.org/10.5194/egusphere-2022-329
Preprint. Discussion started: 20 June 2022

April 2018 and up to 405 mgCH_4 m^{-2} d^{-1} 28 February 2019). During the spring-summer warm up period methane fluxes increased slowly with high peaks of emission, that corresponds to reservoir level changes. The highest annual ebullition and diffusive fluxes registered in the beginning of the autumn convective mixing stage, when the density stratification in water column weakens and disappeared. The reservoir stratification breaks events can occur during the summer warm period as a result of strong wind-waves impact or also with water level drawdown events. In the 2018 and 2019 the beginning of autumn mixing stage and water level drawdowns happens in the same time and the highest values of the flux of all calculation period was registered (649 mgCH_4 m^{-2} d^{-1} 17 October 2018 and 1903 mgCH_4 m^{-2} d^{-1} 17 September 2019). The high temporal variability of the diffusive flux corresponds to methane surface concentration variations, ebullition variations correspond to atmosphere pressure changes.

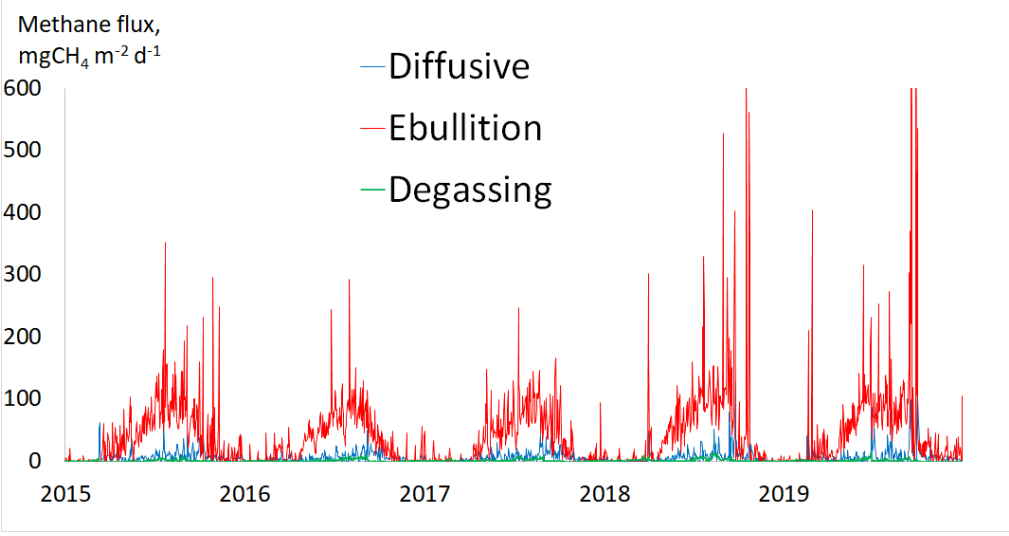

Figure 11: Time series of diffusive, bubble fluxes and degassing through dam into the atmosphere from Mozhaysk reservoir for 2015-2019 simulated by LAKE model

For comparison to the measured total CH_4 flux at station IV, we used the sum of the bubble flux emitted from the second-deepest sediments column in the model ("Soil column 2" at Figure 3), since it most corresponds to the depth below the station IV, and the simulated surface diffusive flux, which is by definition averaged over the reservoir surface (Fig. 12).

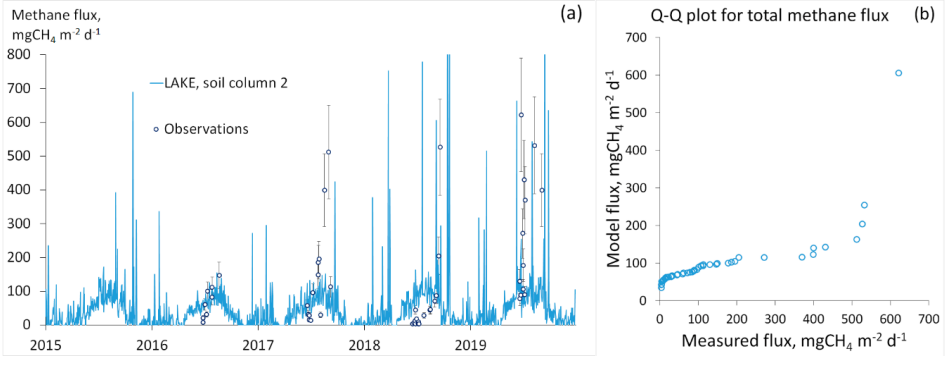

Figure 12. Time series of the total methane flux values for 2015-2019 simulated by the LAKE model (ebullition flux was taken from 2nd sediments column) and according to observations (station IV) (a) and Q-Q plot between in situ measured total methane flux and model simulated total methane flux (b). For observations, values are given at intervals corresponding to the relative error in determining the methane flux into the atmosphere 27 %

https://doi.org/10.5194/egusphere-2022-329
Preprint. Discussion started: 20 June 2022

The main task of using the model is to estimate annual emission, which implies a qualitative reproduction of seasonally averaged emission values, as well as significant methane emission due to mixing of the water column during the destruction of stratification or hydrostatic pressure drops. The model satisfactorily reproduces both background values of the methane flux in the summer period and episodic emissions, which is clearly seen in 2018 and 2019 – the extrema of the flux values according to observations correspond to the peaks according to the model, however, they are shifted in time by 1-2 days. The model results were less successful in the summer of 2017. The methane flux significantly increased during the summer likely due to the accumulation of fresh organic matter at the top of sediments. At the same time, in the model, the temporal variation of methane production in sediments is caused by temperature dynamics only. In the future, it is planned to improve the model by incorporating the variable content of labile organic matter in bottom sediments.

It is noteworthy that oxygen supersaturation in the epilimnion can be a "predictor" for a sharp summer increase in methane emissions, since this supersaturation indicates significant primary production which is not compensated by respiration in the mixed layer, implying rapid removal of dead organic matter from the mixed layer, so that the matter, deposited at the bottom, becomes a substrate for methanogens.

The comparison between annual methane emission estimates by *in situ* measurements and LAKE model presented in Table 8.

Table 8. Annual methane emissions from the Mozhaysk reservoir during 2015-2019 according to the LAKE model simulation and the estimation according to observations

year	Observations			LAKE model			
	Emission from surface, tC-CH_4	Degassing, tC-CH_4	**Total,** tC-CH_4	Diffusive, tC-CH_4	Ebullition, tC-CH_4	Degassing, tC-CH_4	**Total,** tC-CH_4
2015				50.0	287.5	6.5	**344.0**
2016				47.0	268.0	11.4	**326.4**
2017	334	13	**347**	51.7	273.8	11.8	**337.2**
2018	256	9	**265**	52.9	360.8	15.2	**428.9**
2019	378	11	**389**	60.5	354.9	8.9	**424.3**

The annual values of CH_4 fluxes to the atmosphere obtained in the basic run of LAKE model and in measurements are close, excepting for 2018. Most possibly it related to temperature calculation in LAKE model in summer period 2018. Due to high bottom layer temperatures in the model methane generation rate is exceeds the real methane generation rate. The average methane flux from the Mozhaysk reservoir to the atmosphere for the entire simulation period is 34.4 mg C-CH_4 m^{-2} day^{-1} according to field observations and 37.7 mg C-CH_4 m^{-2} day^{-1} according to the model. These values, when compared with global inventories, refer the Mozhaysk reservoir to the upper limit of the emission range for temperate zone (Tortajada et.al., 2012).

The main contribution to the total methane emission according to the LAKE model results makes the ebullition flux, which is especially significant for a large total flux (as mentioned before – during the periods of maximum methane flux into the atmosphere, ebullition can reach up to 95 % of contribution in total flux by model results) (Fig. 11), as well as according to field observations. The tendency of total flux and bubble flux increase starting from the spring period to the end of summer and early autumn with maximal emissions before the autumn convection phase is clearly visible (Fig. 11), which is also consistent with the field measurements. The increase in flux during the warm period in the model is primarily due to an increase of the temperature of bottom water layers and sediments, assuming that methane production is determined by the intensity of microbiological processes that directly depend on the temperature regime.

https://doi.org/10.5194/egusphere-2022-329
Preprint. Discussion started: 20 June 2022

3.2.5. Model sensitivity experiments

An additional model experiment was conducted to assess the sensitivity of the model to changes in the maximum methane oxidation rate in Michaelis-Menthen kinetics. The equation is following (Liikanen et.al., 2002):

$$O = V_{max} \frac{C_{CH_4}}{C_{CH_4} + k_{CH_4}}, \quad (6)$$

where O – methane oxidation rate, C_{CH4} – methane concentration, k_{CH4} – constant of half-saturation for methane oxidation and V_{max} – potential maximum methane oxidation rate.

In this experiment, the maximal reaction rate was doubled from 0.1 mol day^{-1} (as in baseline simulation) to 0.2 mol day^{-1} (Fig. 13). Increase of maximal oxidation rate led to decrease in the mixed-layer CH_4 concentration, bringing in much closer to observed values.

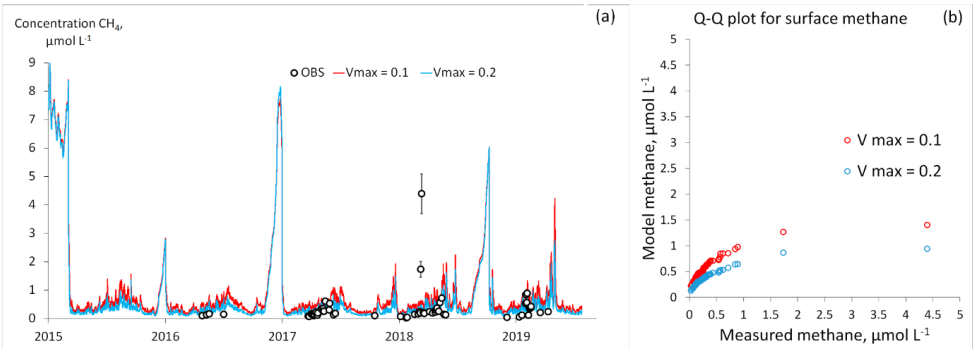

Figure 13. Time series of mixed-layer CH_4 concentration in a baseline numerical experiment with LAKE model (Vmax = 0.1 mol day^{-1}) and an experiment with increased maximal methane oxidation rate (Vmax = 0.2 mol day^{-1}) and Q-Q plot between in situ measured methane concentration and simulated methane concentration for both experiments (b). For observations, values are given at intervals corresponding to the relative error in determining the methane concentration 15.3 %

Table 9 shows different in mean values of methane surface concentration between model experiments and observations.

Table 9. Difference in mean values of methane surface concentration between model calculations and observations

year	Difference in mean, µmolCH_4 L^{-1}	
	Vmax = 0.1	Vmax = 0.2
2016	0.48	0.30
2017	0.28	0.11
2018	0.13	-0.07
2019	0.16	-0.01
All years	0.21	0.02

It is important to note, that changes in methane oxidation equations as constant Vmax, does not affect the ebullition flux, due to bubbles cannot be directly oxidized. Small part of rising bubbles in water column can dissolve and then oxidized, but this is insignificant part of the flux.

The next experiment with model parameters was an experiment with the parameter q10 in methane generation equation in bottom sediments. This parameter determines methane generation multiplier if the temperature increase in 10 °C. The results of these experiments showed on Figure 14. For this figure methane bubble fluxes from model column 2

https://doi.org/10.5194/egusphere-2022-329
Preprint. Discussion started: 20 June 2022

was taken (Fig.3), because the depths of this column closer to depth of station IV, where measurements carried out (Fig. 2).

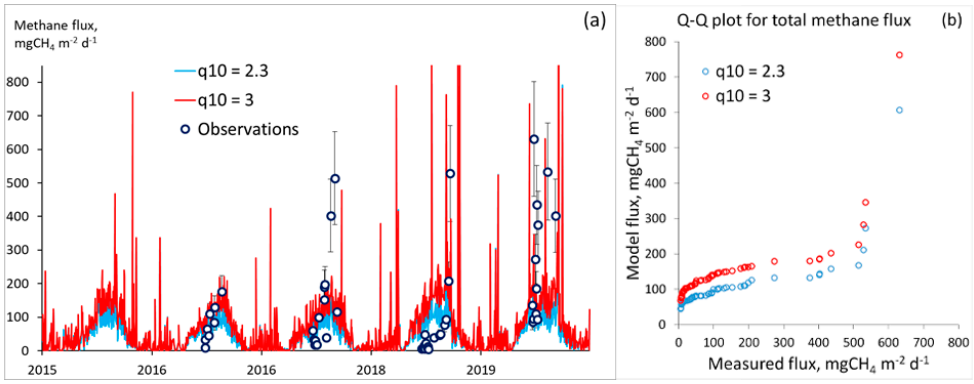

Figure 14. Results of methane fluxes calculation using different values of parameter q10 in comparison with measured values. Bubble fluxes was taken from column 2 of the model bottom sediments columns (a) and Q-Q plot between in situ measured methane total flux and simulated methane flux for both experiments (b). For observations, values are given at intervals corresponding to the relative error in determining the methane flux into the atmosphere 27 %

Parameter q10 is more significant for ebullition calculation, because ebullition is the main contributor of methane emission into the atmosphere. Table 10 shows the difference in mean values between calculated and measured flux.

Table 10. Difference in mean values of methane fluxes into atmosphere between model calculations and observations

year	Difference in mean, mg C-CH_4 m^{-2} day^{-1}	
	q10 = 2.3	q10 = 3.0
2016	-1.8	32.3
2017	-57.7	-27.4
2018	49.6	98.2
2019	-125.8	-77.7
All years	-29.8	10.5

The results of annual methane emissions calculating from the Mozhaysk reservoir based on the results of these two experiments (Vmax = 0.2; q10 = 3) in comparison with regular conditions (Vmax = 0.1 and q10 = 2.3) are shown in Table 11.

Table 11. Methane emission from the Mozhaysk reservoir based on the results of experiments with changes in the potential rate of methane oxidation and the methane generation parameter q10

Year	Emission, tonC-CH_4 Regular conditions	Emission, tonC-CH_4 *Vmax* = 0.2	Emission, tonC-CH_4 *q10* = 3
2015	344	318	443
2016	326	296	447
2017	337	306	430
2018	429	394	555
2019	424	393	528

https://doi.org/10.5194/egusphere-2022-329
Preprint. Discussion started: 20 June 2022

These two parameters – Vmax and q10 can be effectively used for model calibration: Vmax for calibration diffusive emission, q10 – for ebullition. Calibration of these two parameters can give more accurate results of methane emission calculation.

4. Conclusion

Comparison of the LAKE2.3 model results with the observational data showed that the model reproduces the temperature regime of the Mozhaysk reservoir relatively well. The temperature of the bottom water horizons is reproduced significantly worse than the temperature of the epilimnion according to Pearson R and NSE criterias, which is due to the complexity of the vertical heat transfer mechanisms under stable stratification in a reservoir with throughflow, and suggests the development of new background diffusivity parameterization for one-dimensional models better representing the observed mixing. The dissolved oxygen content in the bottom horizons (a very important characteristic for simulation of methane accumulation in hypolimnion) according to the simulation results is very close to the data obtained instrumentally.

The total annual methane emissions from the Mozhaysk reservoir based on field data and model calculations are close. The average flux during the simulation period was 34.4 mgC-CH_4 $m^{-2}day^{-1}$ according to field observations and 37.7 mgC-CH_4 $m^{-2}day^{-1}$ according to the model. This convergence of the results was achieved by calibrating the following parameters: the maximum potential rate of the methane oxidation (an effective parameter for regulating the diffusion flux) and the parameter for temperature dependence of methane production *q10* (shown to be effective for regulating the bubble flux). The bubble component makes the greatest contribution to the total methane flux, in the summer it reaches 95 % of the total flux. The contribution of diffusive, ebullition and degassing fluxes averaged for 5 years of simulations are 52, 309 and 11 tons of methane per year respectively.

The LAKE2.3 model presented in this study can be calibrated using available measurements data at a given reservoir (exemplified in this study by Mozhaysk reservoir) and then used to reproduce the year-round variability of CH_4 flux including the periods where the measurements are not conducted (for example, during the methane release immediately after the ice-off) and thus providing better estimated of annual emission. The model can be used to simulate CH_4 emissions from reservoirs under different approaches to water level management, as well as under contrasting scenarios of future climate change. Numerical experiments of this work demonstrated the key parameters of the model responsible for realistic reproduction of methane fluxes at the water–atmosphere interface and correct assessment of annual emissions from artificial reservoirs.

Acknowledgements. This work is partially supported by the Ministry of Higher Education and Science of Russia (Agreement No. 075-15-2019-1621) and the Grants Council of the President of the Russian Federation (Agreement No. MD-1850.2020.5).

References

1. Aleskerova, A., Kubryakov, A., Stanichny, S.: A two-channel method for retrieval of the Black Sea surface temperature from Landsat-8 measurements, Izvestiya, Atmospheric and Oceanic Physics, 52(9), 1155-1161, 2016
2. Bartosiewicz, M., Ptytulska, A., Laurion, I., Maranger, R.: Effects of phytoplankton blooms on fluxes and emissions of greenhouse gases in a eutrophic lake, Wat. Res., 196, doi:10.1016/j.watres.2021.116985, 2021

https://doi.org/10.5194/egusphere-2022-329
Preprint. Discussion started: 20 June 2022

3. Bastviken, D., Cole, J., Pace, M., Van de Bogert, M.: Fates of methane from different lake habitats: Connecting whole-lake budgets and CH_4 emissions, J. of Geophys. Res, 113, 2024 – 2037, doi:10.1029/2007JG000608, 2008
4. Bastviken, D., Santoro, A., Marotta, H.: Methane emissions from Pantanal, South America, during the low water season: toward more comprehensive sampling, Env. Sci. & tech, 44, 5450 – 5455, doi:10.1021/es1005048, 2010
5. Bazhin, N.: Methane Emission from Bottom Sediments, Chemistry for Sustainable Development, 11, 577 – 580, 2003
6. Beaulieu, J., DelSontro, T., Downing, J.: Eutrophication will increase methane emissions from lakes and impoundments during the 21st century, Nat. comm., 10, 1375 – 1380, https://doi.org/10.1038/s41467-019-09100-5, 2019
7. Borrel, G., Jezequel, D., Bidderre-Petit, C., Morel-Desrosiers, N. et al. Production and consumption of methane in freshwater lake ecosystems, Res. Microbiology, 162, 832 – 847, doi:10.1016/j.resmic.2011.06.004, 2011
8. Businger, J., Wyngaard, J., Izumi, Y., Bradley, E.: Flux-Profile Relationships in the Atmospheric Surface Layer, J. of the Atmos. Sci., 28(2), 181–189, 1971
9. Carrea, L., Embury, O., Merchant, C.J.: Datasets related to in-land water for limnology and remote sensing applications: distance-to-land, distance-to-water, water-body identifier and lake-centre co-ordinates, Geoscience Data Journal, 2, 83 – 97, 2015
10. Deemer, B., Harrison, A., Li, S., Beaulieu, J., et al.: Greenhouse Gas Emissions from Reservoir Water Surfaces: A New Global Synthesis, BioSci, 66(11), 949 – 964, doi:10.1093/biosci/biw117, 2016
11. Donelan, M., Wanninkhof, R.: Gas Transfer at Water Surfaces – Concepts and Issues, Geophys. Monogr. Series, 127, 1–10, doi:10.1029/GM127p0001, 2002
12. Edelshtein, K.: Hydrology of lakes and reservoirs, “Pero” publishing, Moscow, 399 p, 2014 (in Russian)
13. Fichot, C., Miller, W.: An approach to quantify depth-resolved marine photochemical fluxes using remote sensing: Application to carbon monoxide (CO) photoproduction, Remote Sens. of Env., 114(7), 1363–1377, 2010
14. Forster, P., Ramaswamy, V., Artaxo, P., Berntsen, T., et al.: Changes in atmospheric constituents and in Radiative Forcing, Asses. Report of the IPCC, Chapter 2, 129 – 217, 2007
15. Garkusha, D., Fedorova, A., Tambieva, N.: Computing the Methane Cycle Elements in the Aquatic Ecosystems of the Sea of Azov and the World Ocean Based on Empirical Formulae, Russian Meteorology and Hydrology, 41(6), 410 – 417, doi:10.3103/S1068373916060054, 2016
16. Gash, J. (main edit.): Greenhouse gas emissions related to freshwater reservoirs, World Bank Report, UNESCO/IHA GHG Proj., 166 p, 2010
17. Gruca-Rokosz, R., Tomaszek, J.: Methane and Carbon Dioxide in the Sediment of a Eutrophic Reservoir: Production Pathways and Diffusion Fluxes at the Sediment–Water Interface, Water Air & Soil Pollut., 226, 16 – 32, doi:10.1007/s11270-014-2268-3, 2015
18. Guerin, F., Abril, G.: Significance of pelagic aerobic methane oxidation in the methane and carbon budget of a tropical reservoir, J. of Geophys. Res, 112, 3006 – 3020, doi:10.1029/2006JG000393, 2007
19. Guseva, S., Bleninger, T., Jöhnk, K., Polli, B. et al.: Multimodel simulation of vertical gas transfer in a temperate lake, Hydrology and Earth System Sciences, 24, 697–715, http://dx.doi.org/10.5194/hess-24-697-2020, 2020

https://doi.org/10.5194/egusphere-2022-329
Preprint. Discussion started: 20 June 2022

20. Guseva, S., Stepanenko, V., Shurpali, N., Marushchak, M. et al.: Numerical simulation of methane emission from subarctic lake in Komi republic (Russia), GEOGR. ENV. SUSTAIN, 2(9), 58–74, http://dx.doi.org/10.15356/2071-9388/_02v09/_2016/_05, 2016
21. Hanson, P., Pollard, A., Bade, D., Predick, K., et al.: A model of carbon evasion and sedimentation in temperate lakes, Global Change Biology, 10(8), 1285–1298, 2004
22. Harrison, J., Deemer, B., Birchfield, M., O`Malley, M.: Reservoir Water-Level Drawdowns Accelerate and Amplify Methane Emission, Environ. Sci. Technol, 51(3), 1267 – 1277, doi:10.1021/acs.est.6b03185, 2017
23. Harrison, J. A., Prairie, Y. T., Mercier-Blais, S., Soued, C.: Year-2020 Global Distribution and Pathways of Reservoir Methane and Carbon Dioxide Emissions According to the Greenhouse Gas From Reservoirs (G-res) Model. Global Biogeochemical Cycles, 35(6). https://doi.org/10.1029/2020GB006888, 2021
24. Hondzo, M., Stefan, H.: Lake Water Temperature Simulation Model, J. of Hydraulic Engineering, 119(11), 1251 – 1273, 1993
25. Hosoda, K., Murakami, H., Sakaida, F., Kawamura, H.: Algorithm and validation of sea surface temperature observation using MODIS sensors aboard terra and aqua in the western North Pacific, J. of Oceanography, 63(2), 267–280, doi: 10.1007/s10872-007-0027-4, 2007
26. Iakunin, M., Stepanenko, V., Salgado, R., Potes, M., et al.: Numerical study of the seasonal thermal and gas regimes of the largest artificial reservoir in western Europe using the LAKE 2.0 model, Geosci. Mod. Dev., 13(8), 3475–3488, https://doi.org/10.5194/gmd-13-3475-2020, 2020
27. IPCC. The Intergovernmental Panel on Climate Change. https://www.ipcc.ch/, last access: 1 December 2021
28. Ishikawa, M., Gonzalez, W., Golyjeswski, O., Sales, G., Rigotti, J. A., Bleninger, T., Mannich, M., Lorke, A.: Effects of dimensionality on the performance of hydrodynamic models, Geosci. Model Dev., Discuss. [preprint], https://doi.org/10.5194/gmd-2021-250, in review, 2021
29. Kemenes, A., Melack, J., Forsberg, B.: Downstream emissions of CH_4 and CO_2 from hydroelectric reservoirs (Tucuruí, Samuel, and Curuá-Una) in the Amazon basin, Inland Wat., 6, 295 – 302, doi:10.1080/IW-6.3.980, 2016
30. Kiuru, P., Ojala, A., Mammarella, I., Heiskanen, J. et al.: Effects of Climate Change on CO_2 Concentration and Efflux in a Humic Boreal Lake: A Modeling Study, J. of Geophys. Res.: Biogeosci, 123(7), 2212–2233, https://doi.org/10.1029/2018JG004585, 2018
31. Koehler, B., Landelius, T., Weyhenmeyer, G., Machida, N. et al.: Sunlight-induced carbon dioxide emissions from inland waters, Global Biogeochemical Cycles, 28(7), 696–711, 2014
32. Li, S., Zhang, Q.: Carbon emission from global hydroelectric reservoirs revisited, Env. Sci. and pollut. Res. International, 21, 131 – 137, doi: 10.1007/s11356-014-3165-4, 2014
33. Liikanen, A., Murtoniemi, T., Tanskanen, H., Tero, V. et al.: Effects of temperature and oxygen availability on greenhouse gas and nutrient dynamics in sediment of a eutrophic mid-boreal lake, Biogeochemistry, 59(3), 269–286, http://dx.doi.org/10.1023/A%3A1016015526712, 2002
34. Lomov, V., Grechushnikova, M., Kazantsev, V., Repina, I.: Reasons and patterns of spatio-temporal variability of methane emission from the Mozhaysk reservoir in summer period, E3S Web of Conferences IV Vinogradov Conference, 163, 03010, 2020a
35. Lomov, V., Stepanenko, V., Grechushnikova, M., Repina, I.: Methane fluxes in an artificial valley reservoir according to field observations and mathematical modeling, IOP Conf. Ser.: Earth Environ. Sci., 611, 12 – 29, https://doi.org/10.1088/1755-1315/611/1/012029, 2020b

https://doi.org/10.5194/egusphere-2022-329
Preprint. Discussion started: 20 June 2022

36. Louis, V., Kelly, C., Duchemin, E., Rudd, J., et al.: Reservoir surfaces as sources of greenhouse gases to the atmosphere: a global estimate, Bioscience, 50, 766 – 775, doi: 10.1641/0006-3568(2000)050[0766:RSASOG]2.0.CO;2, 2000
37. MacCallum, S.N., Merchant, C.J.: Surface water temperature observations of large lakes by optimal estimation, Canadian Journal of Remote Sensing, 38, 25 – 45, doi: 10.5589/m12-010, 2012
38. McGinnis, D., Greinert, J., Artemov, Y., Beaubien, E., et al.: Fate of rising methane bubbles in stratified waters: How much methane reaches the atmosphere?, J. of Geophys. Res.: Oceans, 111(C9), https://doi.org/10.1029/2005JC003183, 2006
39. Milberg, P., Tornqvist, L., Westerberg, L., Bastviken, D.: Temporal variations in methane emissions from emergentaquatic macrophytes in two boreonemoral lakes, AoB PLANTS, 9, doi:10.1093/aobpla/plx029, 2017
40. Miller, B., Arntzen, E., Goldman, A., Richmond, M.: Methane Ebullition in Temperate Hydropower Reservoirs and Implications for US Policy on Greenhouse Gas Emissions, Env. Manag., 60, 1 – 15, doi:10.1007/s00267-017-0909-1, 2017
41. Nash, J., Sutcliffe, J.: River flow forecasting through conceptual models part I — A discussion of principles, J. of Hydrology, 10(3), 282 – 290, https://doi.org/10.1016/0022-1694(70)90255-6, 1970
42. Ostrovsky, I., McGinnis, D., Lapidus, L., Eckert, W.: Quantifying gas ebullition with echosounder: the role of methane transport by bubbles in a medium-sized lake, Limnol. and Oceanogr.: Methods, 6, 105 – 118, doi:10.4319/lom.2008.6.105, 2008
43. Paulson, C.: The Mathematical Representation of Wind Speed and Temperature Profiles in the Unstable Atmospheric Surface Layer, J. of Applied Meteorology, 9(6), 857–861, 1970
44. Palmer, S.C.J., Kutser, T., Hunter, P.D.: Remote sensing of inland waters: Challenges, progress and future directions, Remote Sens. Environ., 157, 1–8, doi: 10.1016/j.rse.2014.09.021, 2015
45. Rosentreter, J. A., Borges, A. V., Deemer, B. R., Holgerson, M. A., Liu, S., Song, C., et al.: Half of global methane emissions come from highly variable aquatic ecosystem sources, Nature Geoscience, 14(4), 225–230, https://doi.org/10.1038/s41561-021-00715-2, 2021
46. Sadeghian, A., Chapra, S., Hudson, J., Wheater, H., et al.: Improving in-lake water quality modeling using variable chlorophyll a/algal biomass ratios, Environmental Modelling & Software, 101, 73–85, 2018
47. Sanuois, M., Biusquet, P., Poulter, B., Peregon, A., et al.: The global methane budget 2000 – 2012, Earth Syst. Sci. Data, 8, 697 – 751, doi:10.5194/essd-8-697-2016, 2016
48. Schneider, P., Hook, S.J.: Space observations of inland water bodies show rapid surface warming since 1985, Geophysical Research Letters, 37, L22405, doi: 10.1029/2010GL045059, 2010
49. Stefan, H., Fang, X.: Dissolved oxygen model for regional lake analysis, Ecological Modelling, 71(1-3), 37–68, 1994
50. Stepanenko, V., Machul'skaya, E., Glagolev, M., Lykosov, V.: Numerical modeling of methane emissions from lakes in the permafrost zone, Izvestiya - Atmospheric and Oceanic Physics, 47(2), 252–264, http://dx.doi.org/10.1134/S0001433811020113, 2011
51. Stepanenko, V., Mammarella, I., Ojala, A., Miettinen, H., et al.: LAKE 2.0: a model for temperature, methane, carbon dioxide and oxygen dynamics in lakes, Geoscientific Model Development, 9(5), 1977–2006, http://dx.doi.org/10.5194/gmd-9-1977-2016, 2016a

https://doi.org/10.5194/egusphere-2022-329
Preprint. Discussion started: 20 June 2022

52. Stepanenko, V., Repina, I., Ganbat, G., Davaa, G.: Numerical Simulation of Ice Cover of Saline Lakes, Izvestiya, Atmospheric and Oceanic Physics, 55(1), 129–138, https://doi.org/10.1134/S0001433819010092, 2016b
53. Stepanenko, V., Valerio, G., Pilotti, M.: Horizontal pressure gradient parameterization for one-dimensional lake models, J. of Adv. in Modelling Earth Sys., 12, e21063, https://doi.org/10.1029/2019MS001906, 2020
54. Tan, Z., Zhuang, Q.: Arctic lakes are continuous methane sources to the atmosphere under warming conditions, Env. Res. Lett., 10(5), 054016, https://doi.org/10.1088/1748-9326/10/5/054016, 2015
55. Tan, Z., Zhuang, Q., Anthony K.: Modeling methane emissions from arctic lakes: Model development and site-level study, J. of Adv. in Modelling Earth Sys., 7, 459 – 483, doi:10.1002/2014MS000344, 2017a
56. Tan, Z., Zhuang, Q., Shurpali, N., Marushchak, M., et al.: Modeling CO_2 emissions from Arctic lakes: Model development and site-level study, J. of Adv. in Modelling Earth Sys., 9(5), 2190–2213, https://doi.org/10.1002/2017MS001028, 2017b
57. Tikhonov, V.V., Khvostov, I.V., Romanov, A.N., Sharkov, E.A.: Analysis of Changes in the Ice Cover of Freshwater Lakes by SMOS data, Izvestiya, Atmospheric and Oceanic Physics, 54(9), 1135-1140, doi: 10.1134/S0001433818090384, 2018
58. Tortajada, C., Altinbilek, D., Biswas, K.: Impact of large dams: A Global Assessment, Berlin: Springer, 410 p, 2012
59. Tremblay, A., Roehm, C., Varfalvy, L., Garneau, M.: Greenhouse Gas Emissions – Fluxes and Processes, Berlin: Springer, 732 p, 2005
60. Walker, R., Snodgrass, W.: Model for Sediment Oxygen Demand in Lakes, J. of Env. Engineer, 112(1), 25–43, 1986
61. Whiticar, M. J.: The Biogeochemical Methane Cycle, Hydrocarbons, Oils and Lipids: Diversity, Origin, Chemistry and Fate, 78, 669–746, https://doi.org/10.1007/978-3-319-90569-3_5, 2020